BNL-223303-2022-JAAM

# Investigating the Elusive Nature of Atomic O from CO2 Dissociation on Pd(111): The Role of Surface Hydrogen

J. P. Simonovis, A. Hunt

To be published in "JOURNAL OF PHYSICAL CHEMISTRY C"

May 2022

Photon Sciences

**Brookhaven National Laboratory**

**U.S. Department of Energy**

USDOE Office of Science (SC), Basic Energy Sciences (BES) (SC-22)

# DISCLAIMER

# Investigating the Elusive Nature of Atomic O from $CO_2$ Dissociation on Pd(111): The Role of Surface Hydrogen

Juan Pablo Simonovis[1,2], Hong Zhang[3], Ning Rui[2], Adrian Hunt[1], Ivan Orozco[3], Ping Liu[2,3], Sanjaya D. Senanayake[2], Jose A. Rodriguez[2,3], and Iradwikanari Waluyo[1*]

[1] National Synchrotron Light Source II, Brookhaven National Laboratory, Upton, NY 11973

[2] Chemistry Division, Brookhaven National Laboratory, Upton, NY 11973

[3]Department of Chemistry, State University of New York at Stony Brook, Stony Brook, NY 11794

*Corresponding author: iwaluyo@bnl.gov

## Abstract

$CO_2$ dissociation is a key step in $CO_2$ conversion reactions to produce value added chemicals typically through hydrogenation. In many cases, the atomic O produced from $CO_2$ dissociation can potentially block adsorption sites or change the oxidation state of the catalyst. Here we used ambient pressure X-ray photoelectron spectroscopy (AP-XPS) and density functional theory (DFT) calculations to investigate the presence of surface species from the dissociation of $CO_2$ on Pd(111). AP-XPS results show that $CO_2$ was dissociated to produce adsorbed CO, but dissociated atomic O was not observed at room temperature. We were only able to observe atomic O when $CO_2$ was introduced at 500 K. Further investigations of O-covered Pd(111) revealed that chemisorbed O could be easily removed by low pressure of CO and $H_2$. Notably, the effect of $H_2$ is quite prominent since it could react with chemisorbed O at a pressure

as low as $2 \times 10^{-9}$ Torr and the presence of $H_2$ at ambient pressure prevented $CO_2$ dissociation. DFT calculations showed that in the presence of background $H_2$, facile $CO_2$ dissociation took place via the reverse water-gas shift (rWGS) reaction, which resulted in the formation of adsorbed CO and removal of O by $H_2$. DFT also identified the possible variation of surface species on simultaneous exposure of $CO_2$ and $H_2$ over Pd(111) depending on temperature and pressure, which opens alternative opportunities to tune the $CO_2$ hydrogenation catalysis by controlling the reaction conditions.

## Introduction

$CO_2$ hydrogenation is an important reaction to produce value added chemicals such as hydrocarbons and alcohols, as well as to reduce the concentration of this environmentally harmful greenhouse gas in the atmosphere to mitigate the ever-worsening global climate crisis.[1-5] The activation of $CO_2$ on any catalyst surface is an important initial step in $CO_2$ hydrogenation, but it is also often considered difficult due to the inert nature of $CO_2$.[6] Therefore, achieving a detailed understanding of the reaction mechanism of $CO_2$ hydrogenation requires a systematic, fundamental study of the adsorption and activation of $CO_2$ on well-defined model surfaces using theoretical and experimental methods.[6, 7] In particular, the use of in situ techniques is essential at ambient pressure regimes relevant to the reaction conditions, where adsorption/desorption thermodynamics and equilibrium, reaction kinetics, as well the availability of adsorption sites can differ significantly from the idealized ultra-high vacuum conditions.

To this end, numerous ambient pressure X-ray photoelectron spectroscopy (AP-XPS) experiments have been performed to study $CO_2$ dissociation on various well-defined surfaces which can be present in metal/oxide catalysts used for the conversion of the molecule. On Cu(111), $CO_2$ molecularly adsorbs at 0.3 Torr with only a slight dissociation.[8] Cu(100), on the other hand,

was found to be more active in $CO_2$ dissociation at the same pressure, producing atomic O that subsequently poisons the surface and prevents further $CO_2$ adsorption.[8] In another study, this was proposed to be due to the presence of steps.[9] On $TiO_2$(110), $CO_2$ weakly binds to the surface at ambient pressure, but some dissociation does occur, and the resulting atomic *O heals the oxygen vacancies in the oxide lattice.[10, 11] On $CeO_x/TiO_2$(110), $CO_2$ forms surface carbonate and causes the oxidation of $Ti^{3+}$ and $Ce^{3+}$, while the addition of Pt nanoparticles on this mixed oxide surface leads to stronger $CO_2$ binding and the formation of various species, including $CO_3$, CO, C, and $CH_x$.[10] On Pt(111), $CO_2$ dissociation was found to result in the formation of adsorbed CO and atomic O on the surface.[12] The addition of $H_2$ at a 1:1 ratio removes adsorbed atomic O at room temperature, and reverse water-gas shift (RWGS) occurs upon heating.[12] On Ni(111) and Ni(100) surfaces, $CO_2$ adsorption results in the formation of carbonates, adsorbed CO, and graphitic C. NiO was also observed on both surfaces.[13] The formation of carbonates, which is much more dominant on Ni(111) than Ni(100), was explained as due to the reaction between $CO_2$ and atomic O from $CO_2$ dissociation.[13]

As shown from the previous examples, in most cases, $CO_2$ dissociation forms adsorbed CO and inevitably also results in the formation of atomic surface O, which can have detrimental effects, especially when it blocks adsorption sites or change the oxidation state of the surface. On the other hand, when dealing with powders of Pd/ZnO, which are highly active for $CO_2$ hydrogenation to methanol, it has been proposed in several works that the active phase of the catalyst contains a PdZn alloy.[14-19] This suggests that oxygen may not be stable on a Pd-ZnO interface under a hydrogen-rich environment. In this work, we studied $CO_2$ dissociation on the Pd(111) surface using AP-XPS. Although Pd single crystals have been extensively studied for CO oxidation reactions using AP-XPS,[20-23] the behavior of $CO_2$ adsorption and dissociation at ambient

pressure has not been studied. This is important to understand the role of Pd in $CO_2$ activation since, as mentioned above, Pd-based catalysts are quite active for $CO_2$ hydrogenation.[14-19] At low pressure exposures, $CO_2$ neither chemisorbs nor dissociates on Pd(111) or Pd(100) surfaces without the presence of alkali promoters.[24, 25] Calculations based on density functional theory (DFT) found that the $CO_2$ dissociation energy on Pd(111) is among the lowest in a series of single crystal metal surfaces studied.[7] Indeed, at elevated pressure (100 mTorr), our AP-XPS results show that $CO_2$ dissociates on Pd(111) at room temperature, which was revealed by DFT as due to the rWGS reaction in the presence of background $H_2$, resulting in adsorbed CO, but not O. Further investigations revealed that the lifetime of the deposited atomic oxygen depends strongly not only on the presence of CO, but more interestingly also on background $H_2$ gas in the chamber, which likely determines the concentration of atomic H on the surface or in the bulk of palladium. The results of DFT calculations show a complex phase diagram for the coexistence of $CO_2/H_2$ on Pd(111). Minimal pressures of $H_2$ can produce H adatoms which are very efficient for the removal of the O deposited by $CO_2$ dissociation. We report a unique behavior not seen in previous studies that reflects the high affinity that palladium has for hydrogen.

## Experimental and Computational Methods

### Ambient Pressure X-ray Photoelectron Spectroscopy

AP-XPS experiments were conducted at the In Situ and Operando Soft X-ray Spectroscopy (IOS, 23-ID-2) beamline of the National Synchrotron Light Source II (NSLS-II) at Brookhaven National Laboratory (BNL). Further details about the endstation and experimental setup can be found in previous publications[26, 27]. A pyrolytic boron nitride (PBN) heater was used with a type K thermocouple placed between the Pd(111) crystal and the heater. Pd(111) was cleaned by $Ar^+$

sputtering (1 kV at $5 \times 10^{-5}$ Torr Ar) for 20 min, followed by annealing to 1000 K for 5 min, treatment in $2 \times 10^{-7}$ Torr $O_2$ at 800 K for 10 min, and finally flashing the sample to 1000 K. XPS was used to confirm the cleanliness of the surface after several cleaning cycles.

Gases including $CO_2$ (Matheson, ultra-high purity, 99.995%), CO (Matheson, research purity, 99.999%), $O_2$ (Matheson, ultra-high purity, 99.98%), and $H_2$ (Matheson, ultra-high purity, 99.999%) were introduced into the chamber using high precision variable leak valves. A combined hot cathode ion gauge and Pirani gauge was used to read the pressure at 5 mTorr and below, while a capacitance manometer was used above 5 mTorr. Pd 3d and C 1s spectra were measured using a photon energy of 460 eV, and O 1s spectra were measured using a photon energy of 690 eV. The Fermi level at each photon energy was used for energy calibration. To avoid the effect of beam-induced processes, we routinely moved the sample during the experiments, and we performed "dark" experiments (i.e. without X-ray beam) when necessary. XPS spectra were analyzed using CasaXPS. The Tougaard background was applied and a TLA(Gaussian-modified asymmetric) line shape was used for the peak fitting. For the Pd $3p_{3/2}$ spectra, an additional component at ~539 eV was added to account for the plasmon loss peak. Peak fitting parameters such as peak positions and FWHM constraints are provided in Table S1 in the Supporting Information.

**Density Functional Theory Calculations**

To gain a better understanding of surface composition under reaction environment, we used a theoretical model to construct a surface phase diagram for $CO_2$ and $CO_2/H_2$ mixtures on Pd(111). Spin-polarized density functional theory (DFT) calculations were performed using the Vienna Ab initio Simulation Package (VASP)[28-30]. The Perdew-Burke-Ernzerhof (PBE)[31] functional was employed to describe electronic exchange and correlation. The pseudopotential files used were

those prepared by Vaspkit.[32] All systems were initialized using the Conjugate Gradient ionic relaxation algorithm[33] then converged with the RMM-DIIS ionic relaxation algorithm[34] with a plane wave cutoff energy of 400eV. The Brillouin zone was sampled including Γ points. An electronic convergence level of $1 \times 10^{-6}$ eV was employed to obtain convergence of the electronic structure, and ionic relaxation was activated and satisfied until the Hellman-Feynman force was less than 0.02 eV/Å on each ion.

A five-layer (2 × 2) Pd (111) slab was used to model the plain base surface with the bottom two layers frozen to represent the bulk structure underneath. The palladium lattice constant was optimized to be 3.952Å, and 15 Å of vacuum above the surface were used to separate the periodic images of the slabs. The slab model was dipole corrected along the direction of the vacuum.

To map the surface diagram of Pd(111) upon exposure to $CO_2$ and $H_2$, various surface configurations based on Pd(111) were taken into consideration in the DFT calculations. In addition to the plain Pd(111), we have surfaces produced by the partial decomposition of $CO_2$, the dissociation of $H_2$, and those resulted from the reverse water-gas shift (rWGS) reaction ($CO_2 + H_2 \rightarrow CO + H_2O$). Total energies were calculated for surfaces with increasing coverage in monolayer (ML) of dissociated *H (0.25ML, 0.5ML, 0.75ML, 1ML) due to $H_2 + 2* \rightarrow 2*H$, *(O+CO) (0.5ML, 1ML) from $CO_2 + 2* \rightarrow *O + *CO$), *CO (0.25ML, 0.5ML, 0.75ML, 1ML) from $CO_2 + * + H_2 \rightarrow *CO + H_2O$ ) or *O (0.25ML, 0.5ML, 0.75ML, 1ML) from $CO_2 + * \rightarrow CO + *O$ (Figure S1). The individual adsorption tests indicate *H, *O, *CO all prefer FCC sites. In addition, the fully hydrogenated PdH(111) and oxidized PdO(111) surfaces were also calculated by DFT (Figure S1) to capture the possible extreme cases. Finally, possible diffusion of surface *H to the sublayer was considered as well to test the possibility under the experimental condition,

specifically including 0.25ML surface *H diffused to the second layer with the surface covered by 1ML or 0.75ML of *H (Figure S1).

Following previous studies[35-38], the formation Gibbs free energy of each considered surface system is expressed as a function of the chemical potential of gas phase environment of pressures and temperature:

$$\Delta G^f = (G^{sp} + N^{gp} \times \mu^{gp}) - (G^{sr} + N^{gr} \times \mu^{gr})$$

where $G^{sp}$ is the energy of product surface, $N^{gp}$ and $\mu^{gp}$ are the molar amount and chemical potential of gas phase product released. The chemical potential is calculated as $\mu = E_0 + ZPE - TS + \Delta H + RTLn(P/P_0)$, where the free energy ($E_0$) and zero-point energy (ZPE) stay constant and can be calculated by VASP. The additional temperature-dependent entropy (TS) /enthalpy ($\Delta H$) terms and a pressure dependent term ($RTLn(P/P_0)$) can be obtained from NIST-JANAF thermochemical tables [39], $P_0$ is the standard pressure 1 bar. The same terms were applied to the plain surface $G^{sr}$ and reactant gas molecule $\mu^{gr}$. The phase diagram was generated at a certain pressure and temperature of each gas phase involved based on the calculated formation energy $\Delta G^f$.

## Results and Discussion

### AP-XPS Results: Dissociation of $CO_2$ on Pd(111) and H/Pd(111) Surfaces

First, we will discuss the activation of $CO_2$ on Pd(111). Figure 1(a) shows that the Pd $3d_{5/2}$ spectrum of clean Pd(111) in UHV mainly consists of the bulk component at 334.9 eV and the surface component at 334.6 eV. These binding energy values are in agreement with those reported in the literature.[21, 40, 41] There is also a small component at 335.5 eV assigned to surface Pd coordinated to a small amount of adsorbed CO,[21, 40] which is expected to occur at room temperature due to the ever-present background CO in the chamber. This can also be observed from the small

peak at 285.6 eV in the C 1s spectrum (Figure 1(b)). Adsorbed CO is not observed in the O 1s spectrum (Figure 1(c)), possibly due to a time effect since the O 1s spectrum at 690 eV was measured first while the sample was still cooling down after a cleaning cycle, while the C 1s and Pd 3d spectra at 460 eV were measured closer to room temperature. It is also possible that a very small amount of adsorbed CO could not be detected in the O 1s spectrum due to overlap with the Pd $3p_{3/2}$ peak.

Upon exposure to 0.1 mTorr of CO at 300 K, a strong C 1s peak at ~285.8 eV from adsorbed CO appeared. The corresponding O 1s spectrum also shows the peak component for adsorbed CO at 531.1 eV (overlapping with but clearly distinguishable from the Pd $3p_{3/2}$ peak) while the Pd $3d_{5/2}$ spectrum shows the disappearance of the surface Pd component and increased intensity of two components at 335.4 and 335.8 eV (labeled Pd-$CO_A$ and Pd-$CO_B$, respectively). The Pd $3d_{5/2}$ spectrum is in good agreement with those in the literature corresponding to ~0.5 ML CO coverage at 100-120 K, which is the saturation coverage of CO at 300 K.[42] Unlike on Pt(111), the nature of the adsorption sites of CO on Pd(111) is not as well understood, but recent studies have attributed these peaks as due to CO adsorption on a mixture of 3-fold hollow and bridge sites.[40] Particularly, Pd-$CO_A$, which is also observed at low coverages, is assigned to Pd coordinated to one adsorbed CO molecule, while Pd-$CO_B$, which is not present at low coverages, corresponds to Pd coordinated to two adsorbed CO molecules.[40] The Pd $3p_{3/2}$ peak, which overlaps with O 1s, is also slightly shifted to higher binding energy due to CO adsorption.

During AP-XPS experiments, it is not uncommon to observe elevated partial pressures of background gases such as CO due to displacement from chamber walls by gases. Due to the propensity of Pd to bind CO, we need to rule out the adsorption of elevated levels of background CO. C 1s spectrum measured in 1 Torr Ar shows a small increase of adsorbed CO compared to the

clean surface, either due to time effect since at this point the sample temperature had been at 300 K for a longer period of time, or due to a slight displacement of CO from the chamber walls in the presence of Ar. However, the amount of adsorbed CO remained small (<0.01 ML). Therefore, we can rule out any significant adsorption of background CO during ambient pressure experiments.

Upon the introduction of 100 mTorr of $CO_2$, the C 1s peak for adsorbed CO increased significantly to ~0.5 ML, the same as that in 0.1 mTorr CO and much more than the <0.01 ML in 1 Torr Ar, showing that the increased amount of adsorbed CO must have originated from $CO_2$ dissociation and not from background CO. To rule out any possible X-ray induced dissociation, we performed an experiment "in the dark" by exposing the sample to 100 mTorr $CO_2$ without X-ray exposure, followed by pumping down the $CO_2$ and measuring in UHV, and we observed the same adsorbed CO peak at nearly the same intensity (Figure S2). We also observed the same features for adsorbed CO in the O 1s and Pd $3d_{5/2}$ regions, nearly identical to the case in 0.1 mTorr CO. We were also able to reproduce the data with $CO_2$ and CO in separate experiments performed in a different, lab-based AP-XPS instrument (with a Al Kα source), thus confirming our results.

Besides CO, the dissociation of $CO_2$ would also be expected to produce atomic O. On Pd(111), chemisorbed atomic O should appear at ~529.2 eV,[41] which is not observed in Figure 1. On Pt(111), atomic O was clearly observed alongside CO from $CO_2$ dissociation.[12] To investigate the fate of the atomic O, we performed low pressure XPS experiments, and the data are shown in Figure 2. After exposing the surface to $1 \times 10^{-6}$ Torr of $O_2$ at 300 K, we observed chemisorbed O at ~529.2 eV as expected, likely forming a 0.25 ML p(2×2)-O layer.[41] The surface remained clean of adsorbed CO as shown by the nearly flat C 1s spectrum. Upon adding $1 \times 10^{-7}$ Torr CO to the chamber ($O_2$:CO ratio of 10:1), the O 1s peak from chemisorbed O disappeared and the peak from adsorbed CO appeared. This strongly suggests that CO either completely displaced chemisorbed

O due to its strong binding to Pd, or it reacted with O to form $CO_2$, which desorbed immediately. Such a disappearance of the chemisorbed O peak upon the introduction of CO was also observed in a UHV experiment.[41] When we closed the CO leak valve so that only $O_2$ remained in the chamber, only the adsorbed CO peak was observed (albeit at a slightly lower intensity) and the chemisorbed O peak never returned. This shows that the presence of adsorbed CO prevents the adsorption of atomic O on the Pd(111) surface. This could explain why we were not able to see chemisorbed O from $CO_2$ dissociation shown in Figure 1. This is a completely different case from Pt(111), where pre-adsorbed O on the surface was not affected by CO adsorption at similar pressures as in our experiment.[12]

To investigate the presence of CO and O from $CO_2$ dissociation at different temperatures, we performed a series of heating and cooling experiments in the presence of 100 mTorr $CO_2$. The O 1s spectra are shown in Figure 3 while the corresponding C 1s and Pd $3d_{5/2}$ spectra are shown in Figures S3 and S4 in the Supplementary Information. During the heating experiment (Figure 3(a) and Figure S3), we started by introducing 100 mTorr of $CO_2$ at 300 K, then heated the sample stepwise in 50 K increments to 500 K. All peaks associated with adsorbed CO in the C 1s, O 1s, and Pd $3d_{5/2}$ regions gradually decreased in intensity with increasing temperature until eventually it was no longer observed in C 1s and only a small amount was observed in O 1s and Pd $3d_{5/2}$ (the discrepancy here is likely due to a time effect). For Pd 3d, the Pd-$CO_B$ peak (Pd coordinated to two CO molecules) disappeared first at 350 K, leaving the Pd-$CO_A$ peak as the sole component for Pd coordinated to CO. A major difference between heating Pd(111) vs. Pt(111) in $CO_2$ is the accumulation of graphitic C on Pt(111), which was proposed as due to the Boudouard reaction,[12] while we observed no such phenomenon on Pd(111).

For the cooling experiment (Figure 3(b) and Figure S4), we started by heating the sample to 500 K and introduced 100 mTorr of $CO_2$ at 500 K. The O 1s spectrum shows a small shoulder from chemisorbed O at ~529.2 eV, and the Pd $3d_{5/2}$ spectrum shows a small component at 335.5 eV, which can be assigned to Pd coordinated to O atoms, consistent with the literature.[21, 41] Although the binding energy of the Pd-O component is the same as that of the Pd-$CO_A$ peak, it cannot be attributed to adsorbed CO since both the C 1s and O 1s spectra show the absence of CO adsorption at 500 K. We then turned off the heating and let the sample cool down in the presence of $CO_2$. When the sample temperature was around 450 K, the peak from chemisorbed O became more prominent with an estimated coverage of ~0.2 ML, based on the peak area relative to the O(ads) peak in Figure 2(b), spectrum (ii), which is assumed to correspond to the 0.25 ML p(2×2)-O layer. As the sample further cooled down, CO started to adsorb while the chemisorbed O disappeared and could no longer adsorb. This confirmed the effect of CO co-adsorption as we explained previously.

Although the presence of CO can explain the disappearance of chemisorbed O, we further investigated the effect of $H_2$, another common background gas in UHV chamber as well as a reactant in $CO_2$ hydrogenation reaction, on the stability of chemisorbed O. First, we dosed $1 \times 10^{-6}$ Torr of $O_2$ for 10 min to prepare chemisorbed O on the surface, as seen from the O 1s peak at ~529.2 eV in Figure 4. At this point, the sample had been sitting at 300 K for some time, so a small amount of CO had adsorbed on the surface, as observed from the O 1s component at 530.6 eV in Figures 4(a). This small amount of adsorbed background CO was not enough to react with or displace chemisorbed O. Then, we pumped down the $O_2$ and introduced a very low pressure of $H_2$ ($2 \times 10^{-9}$ Torr above the base pressure of the chamber). After 1 minute of data acquisition in this pressure of $H_2$, the O 1s peak from chemisorbed O decreased by a factor of two, and after 5

minutes, it was completely removed. This shows the reactive nature of chemisorbed O on Pd(111) since it is highly susceptible to reaction even with a low pressure of $H_2$ in the background. To rule out beam-induced effects, we performed experiments without $H_2$ with extended X-ray exposure as well as with $H_2$ without X-ray exposure, shown in Figure 4(b). Exposure of the chemisorbed O to X-ray beam in UHV for up to 15 min resulted only in a slight intensity decrease, but after we exposed the sample to $2 \times 10^{-9}$ Torr of $H_2$ without X-ray exposure, followed by pumping down the $H_2$, the chemisorbed O peak disappeared. This unambiguously shows that $H_2$ was responsible for removing O from the Pd(111) surface and that the X-ray beam had an insignificant effect. It should be noted that more CO had adsorbed from the background during the experiment, but the small amount played no role in displacing O. In this case, the low pressure of $H_2$ had a stronger effect than adsorbed CO in removing O.

Finally, we examine the effect of the co-presence of $CO_2$ and $H_2$ at ambient pressure to simulate $CO_2$ hydrogenation conditions. Figure 5(a) shows that in 0.9 Torr of $H_2$ (spectrum (ii)), only a small amount (<0.01 ML) of adsorbed background CO was observed in the C 1s region, again showing that ambient pressure experiments did not significantly increase the partial pressure of background CO. The Pd $3d_{5/2}$ spectrum (Figure 5(b)) shows a large shift to higher binding energy, reminiscent of that from CO adsorption and $CO_2$ dissociation shown in Figure 1(c), but the small amount of adsorbed CO in C 1s indicated this particular shift must have been from adsorbed H from $H_2$ dissociation. The nature of H adsorption sites on Pd(111) is not the focus of this paper, so we only fitted the spectrum with one peak attributed to Pd-H and we will not attempt to discuss this in detail in this paper. Upon introducing 0.1 Torr of $CO_2$ to the 0.9 Torr of $H_2$ already present in the chamber (spectrum (iii)), we did not see any significant changes in the spectra, indicating that no $CO_2$ dissociation took place. To confirm the effect of $H_2$, we performed an

experiment with 1 Torr of Ar introduced first into the chamber followed by 0.1 mTorr of $CO_2$ (spectrum (iv)), with switching the order of $CO_2$ and $H_2$ dosing (i.e. 0.1 mTorr of $CO_2$ first, followed by 0.9 Torr of $H_2$, spectrum (v)), and 0.9 Torr of $H_2$ followed by a small amount of CO (spectrum (vi), the CO pressure was low enough that it did not register on the gauge reading on top of the 0.9 Torr of $H_2$, but we can estimate it very roughly to be less than $1 \times 10^{-3}$ Torr). As shown in Figure 5(a), the $CO_2$-first experiment (v) resulted in a large CO peak, identical to the case of $CO_2$ on its own (Figure 1). This shows that $CO_2$ dissociation proceeded as expected before ambient pressure of $H_2$ was introduced and the higher pressure of $H_2$ that followed had no effect of displacing or reacting with the produced CO at room temperature. The O 1s peak of chemisorbed O was, unsurprisingly, not observed due to the presence of CO and $H_2$. With the presence of 1 Torr of Ar already in the chamber (iv), $CO_2$ dissociation still occurred, but the resulting CO peak was smaller (~0.17 ML, estimated from the peak area relative to the ~0.5 ML saturation coverage in Figure 1(b)) than that from $CO_2$ on its own or the $CO_2$+ $H_2$ experiment for the same exposure time (~0.5 ML). This is likely because the presence of gas phase Ar reduced the rate of impingement of $CO_2$ on the surface, thereby decreasing the reaction rate. However, as an inert gas, Ar cannot form strong chemical interactions with Pd, so it did not prevent $CO_2$ activation. For the $H_2$+CO experiment (vi), CO at low pressure could readily adsorb in the presence of excess $H_2$, so the presence of adsorbed H on the surface did not have any effect on CO adsorption. On the other hand, for the $H_2$+ $CO_2$ experiment, the fact that we did not see adsorbed CO from $CO_2$ dissociation and that the adsorbed H remained intact (Figure 5(b)) likely suggests that the Pd-H interaction at ambient pressure was strong enough to prevent $CO_2$ dissociation. It should be noted that after we performed experiments at ambient pressure of $H_2$, we were not able to see chemisorbed O from $CO_2$ dissociation again on the surface, even if we tried to replicate the cooling experiment shown

in Figure 3(b). This is likely due to the higher partial pressure of $H_2$ in the chamber after an ambient pressure experiment, which, as we showed in Figure 4, can easily remove O, unless we performed an extended bake-out of the chamber.

**DFT Results: Phase Diagrams for Exposure of Pd(111) to $CO_2$/$H_2$ Mixtures**

The experimental results described in the previous section indicate that low pressures of $H_2$ present in the XPS chamber can have a tremendous influence on the stability of O chemisorbed on Pd(111) and the surface chemistry associated with the dissociation of $CO_2$. Phase diagrams as a function of the partial pressures of $CO_2$ and $H_2$ on Pd(111) at 300 K (Figure 6(a)) and 500 K (Figure 6(b)) were determined based on DFT-calculated total energies and data from NIST-JANAF thermochemical tables (Tables S2 and S3). The corresponding structures of each surface phase are displayed in Figure 7. The CO reservoir was treated as constant because experimentally the system was pumped down to UHV level ($2 \times 10^{-9}$ Torr) before exposing the sample to $CO_2$ and $H_2$. We approximated the partial pressure of CO at $10^{-12}$ bar, which is equivalent to $7.5 \times 10^{-10}$ Torr. As shown in Figure 6, at both 300 and 500 K, Pd(111) is the most stable at low pressure of $CO_2$ and $H_2$. With the increasing $H_2$ partial pressure along the Y-axis, the surface prefers to be partially and fully covered by *H, eventually transforming to PdH(111). With the increasing $CO_2$ pressure along the X-axis, Pd(111) favors to be gradually covered by *CO.

Under a condition of 300 K and $H_2$ partial pressure of $7.5 \times 10^{-10}$ Torr (simulating $H_2$ from the background, after pumping down to UHV), Pd(111) is likely to be partially covered by *H, shown in Figures 6(a). Upon the exposure to $CO_2$ with a partial pressure of 0.1 Torr, the surface favors the formation of Pd(111) covered by 0.5ML of *CO, *$CO_{0.5ML}$/Pd(111) shown in Figures 6(a) and 7. That is, only *CO remained on the surface upon exposure to $CO_2$, which is in agreement

with AP-XPS observations (Figure 1). We also considered to exclude the possible interaction between background $H_2$ and $CO_2$ (Figure S5), in which case *CO does not form on the Pd(111) surface. The same situation is observed at a $H_2$ pressure below ~$10^{-15}$ Torr at 300 K, under which the $H_2$ level is too low to allow the formation of *H on the surface, and Pd(111) rather than *H/Pd(111) is stable (Figure 6(a)). This shows that the presence of low pressures of $H_2$ promotes the activation of $CO_2$ and removal of *O from $CO_2$ via the rWGS reaction, $CO_{2(g)}$ + 2 *H → *CO + $H_2O_{(g)}$, which is exothermic with energy release of 0.81eV and is likely to proceed well at 300 K. The co-adsorption of *O and *CO from the direct dissociation of $CO_2$, $CO_{2(g)}$ + 2* → *CO + *O, is possible, but it requires an extremely high $CO_2$ pressure ($10^{18}$ Torr) to achieve. This is due to the endothermicity of $CO_2$ dissociation with energy cost of 0.69 eV per molecule, which is less favorable than that of rWGS reaction with the presence of $H_2$.

The heating experiment indicated the desorption of *CO at elevated temperatures (Figure 3). Indeed, theoretically *$CO_{0.5ML}$/Pd(111) (Figure 6(a)) is shown to transform to Pd(111) by raising the temperature from 300 K to 500 K under the same $CO_2$ and $H_2$ exposure (Figures 6(b) and 7). That is, all surface *CO species are not stable and prefer to desorb at 500K, which agrees with the XPS measurement. In addition, such a temperature-driven destabilization was also observed for *H, where at $H_2$ partial pressure of $7.5 \times 10^{-10}$ Torr from background, Pd(111) remains intact rather than the partially *H-covered as seen for the case at 300 K (Figure 6). Interestingly, without the presence of *H, chemisorbed *O is only observed at high $CO_2$ pressure (~$10^{10}$ Torr, Figure 6(b)). In this case the adsorbed *CO from $CO_2$ dissociation desorbs, and only the atomic *O is left on the surface due to the lack of *H. The removal of *O as water is enabled by lowering the temperature and thus regeneration of *H. Such sequence described the XPS results well (Figure 3). Specifically, by the exposure of Pd(111) at 500 K to 0.1 Torr of $CO_2$, the chemisorbed *O was

observed, which disappeared at lower temperature. The only difference is that the $CO_2$ pressure required for formation of *O is much lower in experiment than that in theory. This may be associated with the presence of low-coordinated steps, kinks or defective Pd sites in the experiment, which was reported to provide much stronger binding than the high-coordinated sites on ideal Pd(111) modeled in theory[43].

In the scenario of sequential exposure to 0.9 Torr of $H_2$ first and then 0.1 Torr of $CO_2$ at 300K (Figure 5), Pd(111) prefers to be covered by 1 ML of hydrogen or $*H_{1ML}$/Pd(111), after the first exposure (Figures 6(a) and 7). However, the $CO_2$ dissociation was found to be prohibited by surface *H on $H_{1ML}$/Pd(111), in agreement with the experimental observations (Figure 5).

**Conclusions**

By combining experimental results from AP-XPS and computational results from DFT, we studied the dissociation of $CO_2$ on Pd(111) with a focus on investigating the fate of the resulting atomic O. While adsorbed CO was observed from the room-temperature dissociation of $CO_2$ at ambient pressure, chemisorbed O was only observed under a condition in which the sample was already at 500 K when $CO_2$ was introduced. We studied the interaction of chemisorbed O with CO and $H_2$ at low pressures and found that O was readily displaced by CO even when $O_2$ was in excess and more interestingly, O easily reacted with $H_2$ at a pressure of as low as $2 \times 10^{-9}$ Torr, just slightly higher than the chamber base pressure. In addition, $CO_2$ dissociation could not occur in ambient pressure of $H_2$.

The DFT calculations described well the experimental observations found during the exposure of Pd(111) to $CO_2$. Specifically, DFT shows that $CO_2$ dissociation to form *CO proceeded through the rWGS reaction assisted by the presence of background $H_2$, which facilitated

removal of *O by $H_2$. DFT also confirmed the heating/cooling behaviors in the presence of $CO_2$, as well as the hindered $CO_2$ dissociation on Pd(111) by the presence of ambient pressure of $H_2$. In addition, the calculations revealed a strong dependence of the surface phase and thus the catalysis of $CO_2$ hydrogenation on Pd(111) on the pressure of $H_2/CO_2$ and temperature, including Pd(111), *H-covered Pd(111), *CO-covered Pd(111), and PdH(111). Our study provides alternative opportunities to tune the selectivity for $CO_2$ hydrogenation on Pd by controlling the $CO_2/H_2$ exposure cycles.

**Supporting Information available**

Examples of surface models used in DFT calculations; C 1s spectra for $CO_2$ adsorption with and without X-ray beam, C 1s and Pd $3d_{5/2}$ AP-XPS spectra during heating and cooling in $CO_2$; DFT-calculated Pd(111) phase diagram without reverse water-gas shift; table of XPS fitting parameters, table of DFT-calculated energy of each surface phase.

**Acknowledgements**

This research used resources of the 23-ID-2 (IOS) beamline of the National Synchrotron Light Source II, a U.S. Department of Energy (DOE) Office of Science User Facility operated for the DOE Office of Science by Brookhaven National Laboratory under Contract No. DE-SC0012704. The research done at the BNL Chemistry Division was supported by the division of Chemical Science, Geoscience, and Bioscience, Office of Basic Energy Science of the US Department of Energy (DOE) under Contract No. DE-SC0012704. DFT calculations in this work were performed using computational resources at Center for Functional Nanomaterials (CFN), and the Scientific Data and Computing Center, a component of the Computational Science Initiative, at BNL under

Contract No. DE-SC0012704, and at Stony Brook University, which was founded by National Science Foundation grant (#1531492).

**References**

1. Karl, T. R.; Trenberth, K. E., Modern Global Climate Change. *Science* **2003,** *302*, 1719-1723.

2. Aresta, M., *Carbon Dioxide as Chemical Feedstock*. Wiley-VCH: Weinheim, Germany, **2010**.

3. Song, C. S., Global Challenges and Strategies for Control, Conversion and Utilization of $CO_2$ for Sustainable Development Involving Energy, Catalysis, Adsorption and Chemical Processing. *Catal. Today* **2006,** *115*, 2-32.

4. Meinshausen, M.; Meinshausen, N.; Hare, W.; Raper, S. C. B.; Frieler, K.; Knutti, R.; Frame, D. J.; Allen, M. R., Greenhouse-Gas Emission Targets for Limiting Global Warming to 2 °C. *Nature* **2009,** *458*, 1158-1162.

5. Centi, G.; Quadrelli, E. A.; Perathoner, S., Catalysis for $CO_2$ Conversion: A Key Technology for Rapid Introduction of Renewable Energy in the Value Chain of Chemical Industries. *Energ. Environ. Sci.* **2013,** *6*, 1711-1731.

6. Freund, H. J.; Roberts, M. W., Surface Chemistry of Carbon Dioxide. *Surf. Sci. Rep.* **1996,** *25*, 225-273.

7. Liu, X. J.; Sun, L.; Deng, W. Q., Theoretical Investigation of $CO_2$ Adsorption and Dissociation on Low Index Surfaces of Transition Metals. *J. Phys. Chem. C* **2018,** *122*, 8306-8314.

8. Eren, B.; Weatherup, R. S.; Liakakos, N.; Somorjai, G. A.; Salmeron, M., Dissociative Carbon Dioxide Adsorption and Morphological Changes on Cu(100) and Cu(111) at Ambient Pressures. *J. Am. Chem. Soc.* **2016,** *138*, 8207-8211.

9. Hagman, B.; Posada-Borbon, A.; Schaefer, A.; Shipilin, M.; Zhang, C.; Merte, L. R.; Hellman, A.; Lundgren, E.; Grönbeck, H.; Gustafson, J., Steps Control the Dissociation of $CO_2$ on Cu(100). *J. Am. Chem. Soc.* **2018,** *140*, 12974-12979.

10. Grinter, D. C.; Graciani, J.; Palomino, R. M.; Xu, F.; Waluyo, I.; Sanz, J. F.; Senanayake, S. D.; Rodriguez, J. A., Adsorption and Activation of $CO_2$ on Pt/$CeO_x$/$TiO_2$(110): Role of the Pt-$CeO_x$ Interface. *Surf. Sci.* **2021,** *710*, 121852.

11. Hamlyn, R. C. E.; Mahapatra, M.; Grinter, D. C.; Xu, F.; Luo, S.; Palomino, R. M.; Kattel, S.; Waluyo, I.; Liu, P.; Stacchiola, D. J., et al., Imaging the Ordering of a Weakly Adsorbed Two-Dimensional Condensate: Ambient-Pressure Microscopy and Spectroscopy of $CO_2$ Molecules on Rutile $TiO_2$(110). *Phys. Chem. Chem. Phys.* **2018,** *20*, 13122-13126.

12. Su, H. Y.; Ye, Y. F.; Lee, K. J.; Zeng, J.; Mun, B. S.; Crumlin, E. J., Probing the Surface Chemistry for Reverse Water Gas Shift Reaction on Pt(111) Using Ambient Pressure X-Ray Photoelectron Spectroscopy. *J. Catal.* **2020,** *391*, 123-131.

13. Cai, J.; Han, Y.; Chen, S. Y.; Crumlin, E. J.; Yang, B.; Li, Y. M.; Liu, Z., $CO_2$ Activation on Ni(111) and Ni(100) Surfaces in the Presence of $H_2O$: An Ambient-Pressure X-Ray Photoelectron Spectroscopy Study. *J. Phys. Chem. C* **2019,** *123*, 12176-12182.

14. Iwasa, N.; Suzuki, H.; Terashita, M.; Arai, M.; Takezawa, N., Methanol Synthesis from $CO_2$ under Atmospheric Pressure over Supported Pd Catalysts. *Catal. Lett.* **2004,** *96*, 75-78.

15. Bahruji, H.; Bowker, M.; Hutchings, G.; Dimitratos, N.; Wells, P.; Gibson, E.; Jones, W.; Brookes, C.; Morgan, D.; Lalev, G., Pd/ZnO Catalysts for Direct $CO_2$ Hydrogenation to Methanol. *J. Catal.* **2016,** *343*, 133-146.

16. Fan, L.; Fujimoto, K., Promotive SMSI Effect for Hydrogenation of Carbon Dioxide to Methanol on a Pd/$CeO_2$ Catalyst. *J. Catal.* **1994,** *150*, 217-220.

17. Collins, S. E.; Chiavassa, D. L.; Bonivardi, A. L.; Baltanas, M. A., Hydrogen Spillover in $Ga_2O_3$-Pd/$SiO_2$ Catalysts for Methanol Synthesis from $CO_2$/$H_2$. *Catal. Lett.* **2005,** *103*, 83-88.

18. Ye, J. Y.; Liu, C. J.; Mei, D. H.; Ge, Q. F., Methanol Synthesis from $CO_2$ Hydrogenation over a $Pd_4$/$In_2O_3$ Model Catalyst: A Combined DFT and Kinetic Study. *J. Catal.* **2014,** *317*, 44-53.

19. Jiang, X.; Koizumi, N.; Guo, X. W.; Song, C. S., Bimetallic Pd-Cu Catalysts for Selective $CO_2$ Hydrogenation to Methanol. *Appl. Catal. B-Environ.* **2015,** *170*, 173-185.

20. Toyoshima, R.; Yoshida, M.; Monya, Y.; Kousa, Y.; Suzuki, K.; Abe, H.; Mun, B. S.; Mase, K.; Amemiya, K.; Kondoh, H., In Situ Ambient Pressure XPS Study of CO Oxidation Reaction on Pd(111) Surfaces. *J. Phys. Chem. C* **2012,** *116*, 18691-18697.

21. Schiller, F.; Ilyn, M.; Perez-Dieste, V.; Escudero, C.; Huck-Iriart, C.; del Arbol, N. R.; Hagman, B.; Merte, L. R.; Bertram, F.; Shipilin, M., et al., Catalytic Oxidation of Carbon Monoxide on a Curved Pd Crystal: Spatial Variation of Active and Poisoning Phases in Stationary Conditions. *J. Am. Chem. Soc.* **2018,** *140*, 16245-16252.

22. Yu, Y.; Kim, D.; Lim, H.; Kim, G.; Koh, Y. E.; Kim, D.; Ueda, K.; Hiwasa, S.; Mase, K.; Bournel, F., et al., Operando Study of Pd(100) Surface During CO Oxidation Using Ambient Pressure X-Ray Photoemission Spectroscopy. *AIP Adv.* **2019,** *9*, 015314.

23. Blomberg, S.; Zetterberg, J.; Gustafson, J.; Zhou, J.; Brackmann, C.; Lundgren, E., Comparison of AP-XPS and PLIF Measurements During CO Oxidation over Pd Single Crystals. *Top. Catal.* **2016,** *59*, 478-486.

24. Ehrlich, D.; Wohlrab, S.; Wambach, J.; Kuhlenbeck, H.; Freund, H. J., Reaction of $CO_2$ on Pd(111) Activated Via Promotor Action of Alkali Coadsorption. *Vacuum* **1990,** *41*, 157-160.

25. Wambach, J.; Odörfer, G.; Freund, H. J.; Kuhlenbeck, H.; Neumann, M., Influence of Alkali Co-adsorption on the Adsorption and Reaction of $CO_2$ on Pd(111). *Surf. Sci.* **1989,** *209*, 159-172.

26. Simonovis, J. P.; Hunt, A.; Palomino, R. M.; Senanayake, S. D.; Waluyo, I., Enhanced Stability of Pt-Cu Single-Atom Alloy Catalysts: In Situ Characterization of the Pt/Cu(111) Surface in an Ambient Pressure of CO. *J. Phys. Chem. C* **2018,** *122*, 4488-4495.

27. Simonovis, J. P.; Hunt, A.; Senanayake, S. D.; Waluyo, I., Subtle and Reversible Interactions of Ambient Pressure $H_2$ with Pt/Cu(111) Single-Atom Alloy Surfaces. *Surf. Sci.* **2019,** *679*, 207-213.

28. Kresse, G.; Furthmüller, J., Efficient Iterative Schemes for Ab Initio Total-Energy Calculations Using a Plane-Wave Basis Set. *Phys. Rev. B Condens. Matter* **1996,** *54*, 11169-11186.

29. Kresse, G.; Joubert, D., From Ultrasoft Pseudopotentials to the Projector Augmented-Wave Method. *Phys. Rev. B* **1999,** *59*, 1758-1775.

30. Kresse, G.; Furthmüller, J., Efficiency of Ab-Initio Total Energy Calculations for Metals and Semiconductors Using a Plane-Wave Basis Set. *Comput. Mater. Sci.* **1996,** *6*, 15-50.

31. Perdew, J. P.; Burke, K.; Ernzerhof, M., Generalized Gradient Approximation Made Simple. *Phys. Rev. Lett.* **1996,** *77*, 3865-3868.

32. Wang, V.; Xu, N.; Liu, J.-C.; Tang, G.; Geng, W.-T., VASPKIT: A User-Friendly Interface Facilitating High-Throughput Computing and Analysis Using VASP Code. *Comput. Phys. Commun.* **2021,** *267*, 108033.

33. Press, W. H.; Flannery, B. P.; Teukolsky, S. A.; Vetterling, W. T., *Numerical Recipes: The Art of Scientific Computing*. Cambridge University Press: New York, **1986**.

34. Pulay, P., Convergence Acceleration of Iterative Sequences. The Case of SCF Iteration. *Chem. Phys. Lett.* **1980,** *73*, 393-398.

35. Yu, L.; Liu, Y.; Yang, F.; Evans, J.; Rodriguez, J. A.; Liu, P., CO Oxidation on Gold-Supported Iron Oxides: New Insights into Strong Oxide–Metal Interactions. *J. Phys. Chem. C* **2015,** *119*, 16614-16622.

36. Duan, Z.; Henkelman, G., CO Oxidation on the Pd(111) Surface. *ACS Catalysis* **2014,** *4*, 3435-3443.

37. Rogal, J.; Reuter, K.; Scheffler, M., CO Oxidation at Pd(100): A First-Principles Constrained Thermodynamics Study. *Phys. Rev. B* **2007,** *75*, 205433.

38. Svenum, I.-H.; Herron, J. A.; Mavrikakis, M.; Venvik, H. J., $Pd_3Ag(111)$ as a Model System for Hydrogen Separation Membranes: Combined Effects of CO Adsorption and Surface Termination on the Activation of Molecular Hydrogen. *Top. Catal.* **2020,** *63*, 750-761.

39. Chase, M. W., Jr., *NIST-JANAF Thermochemical Tables, 4th Edition*. J. Phys. Chem. Ref. Data Monograph No. 9; **1998**.

40. Martin, N. M.; Van den Bossche, M.; Grönbeck, H.; Hakanoglu, C.; Zhang, F.; Li, T.; Gustafson, J.; Weaver, J. F.; Lundgren, E., CO Adsorption on Clean and Oxidized Pd(111). *J. Phys. Chem. C* **2014,** *118*, 1118-1128.

41. Leisenberger, F. P.; Koller, G.; Sock, M.; Surnev, S.; Ramsey, M. G.; Netzer, F. P.; Klötzer, B.; Hayek, K., Surface and Subsurface Oxygen on Pd(111). *Surf. Sci.* **2000,** *445*, 380-393.

42. Surnev, S.; Sock, M.; Ramsey, M. G.; Netzer, F. P.; Wiklund, M.; Borg, M.; Andersen, J. N., CO Adsorption on Pd(111): A High-Resolution Core Level Photoemission and Electron Energy Loss Spectroscopy Study. *Surf. Sci.* **2000,** *470*, 171-185.

43. Xu, L.; Bhandari, S.; Chen, J.; Glasgow, J.; Mavrikakis, M., Chloroform Hydrodechlorination on Palladium Surfaces: A Comparative DFT Study on Pd(111), Pd(100), and Pd(211). *Top. Catal.* **2020,** *63*, 762-776.

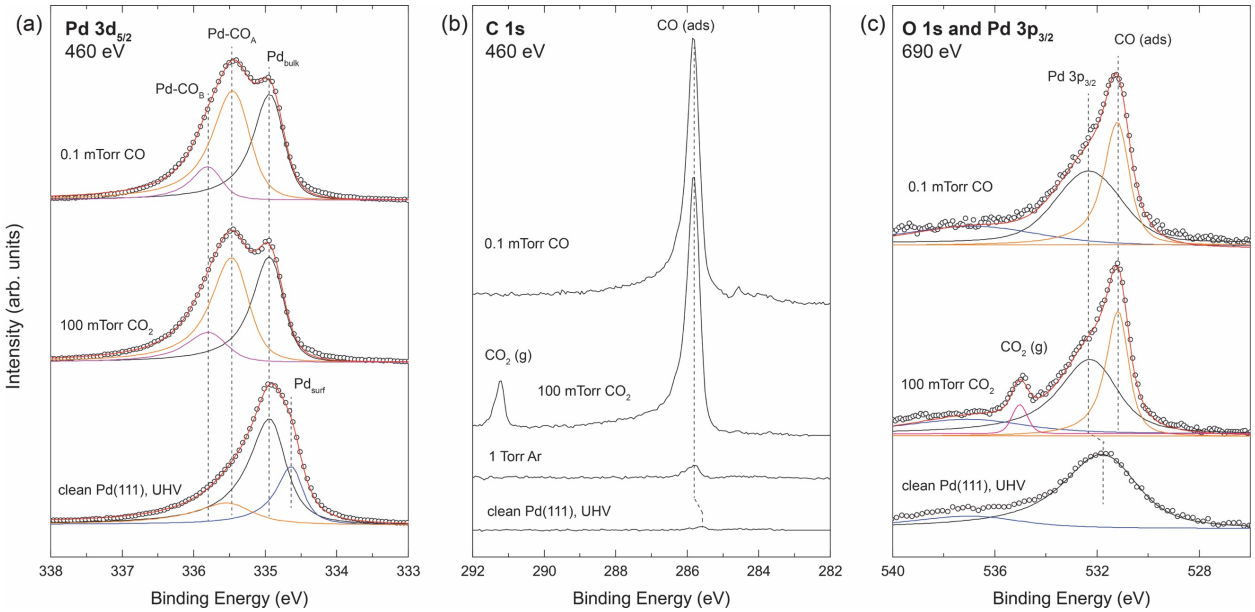


**Figure 1.** (a) Pd $3d_{5/2}$, (b) C 1s, and (c) O 1s and Pd $3p_{3/2}$ XPS spectra of Pd(111) under each indicated experimental condition. All spectra were acquired at ~300 K. For (a) and (c), the open circles represent the experimental data while the solid lines are the fits.

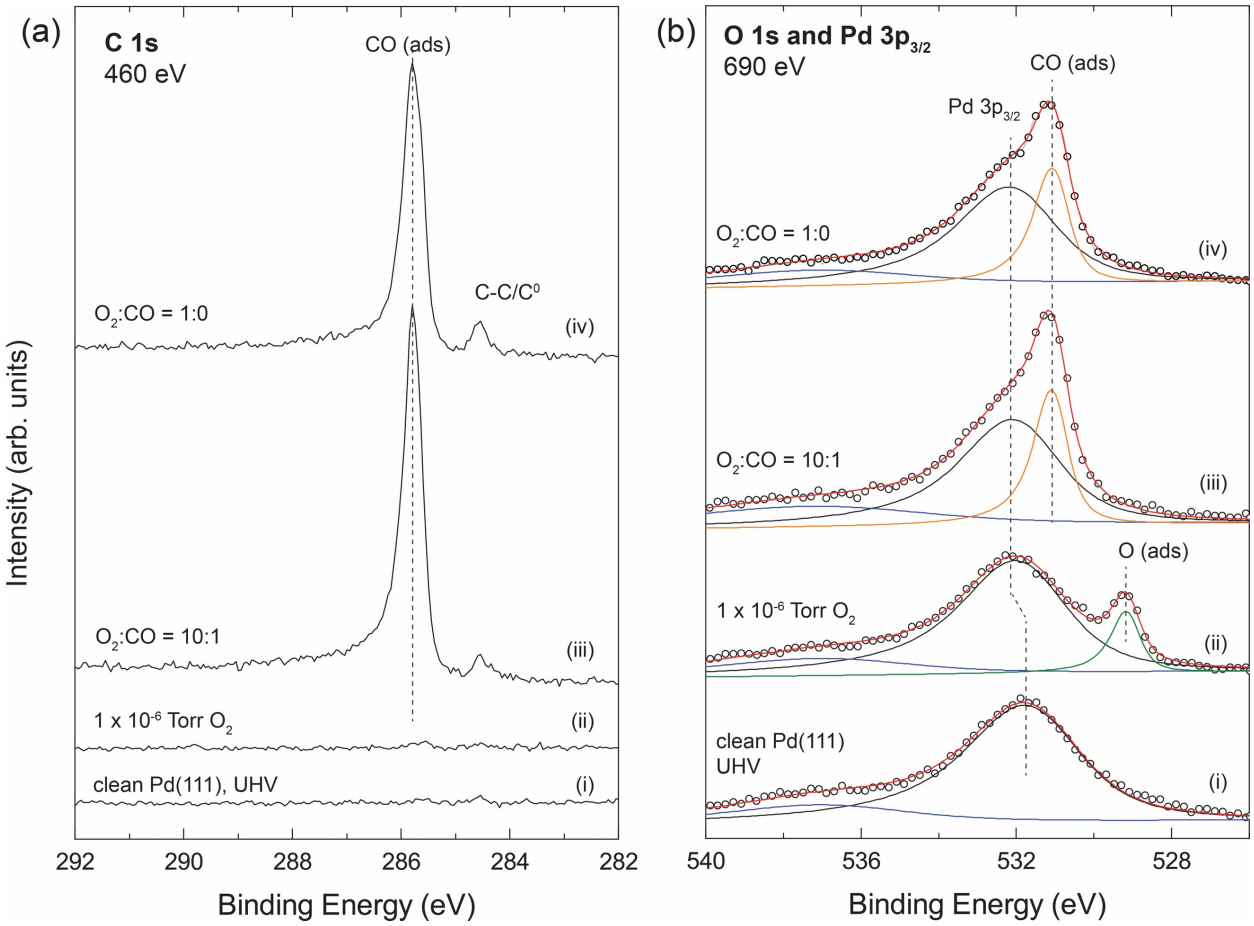


**Figure 2.** (a) C 1s and (b) O 1s/Pd $3p_{3/2}$ XPS spectra of (i) the initial clean Pd(111) in UHV, (ii) after introducing $1 \times 10^{-6}$ Torr $O_2$ to prepare chemisorbed atomic O, followed by (iii) adding 1 x $10^{-7}$ Torr of CO to $1 \times 10^{-6}$ Torr of $O_2$ already in the chamber, and (iv) finally pumping down CO so that only $1 \times 10^{-6}$ Torr of $O_2$ remained in the chamber. In (b), the open circles represent the experimental data while the solid lines are the fits.

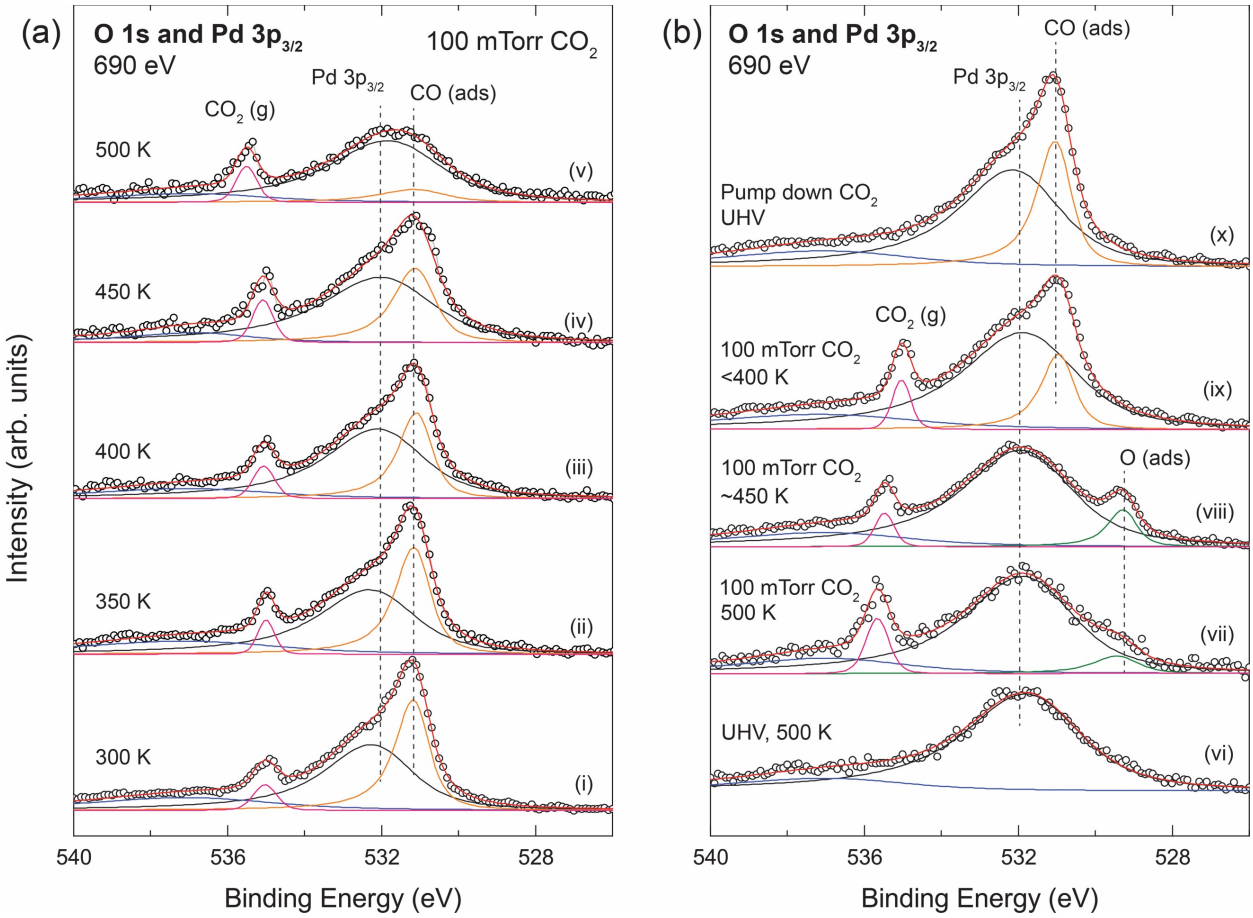


**Figure 3.** O 1s / Pd $3p_{3/2}$ XPS spectra of Pd(111) during (a) heating and (b) cooling in 100 mTorr of $CO_2$ (experimental sequence is (i) to (v) for heating and (vi) to (x) for cooling). The cooling experiment started and ended in UHV. The open circles represent the experimental data while the solid lines are the fits.

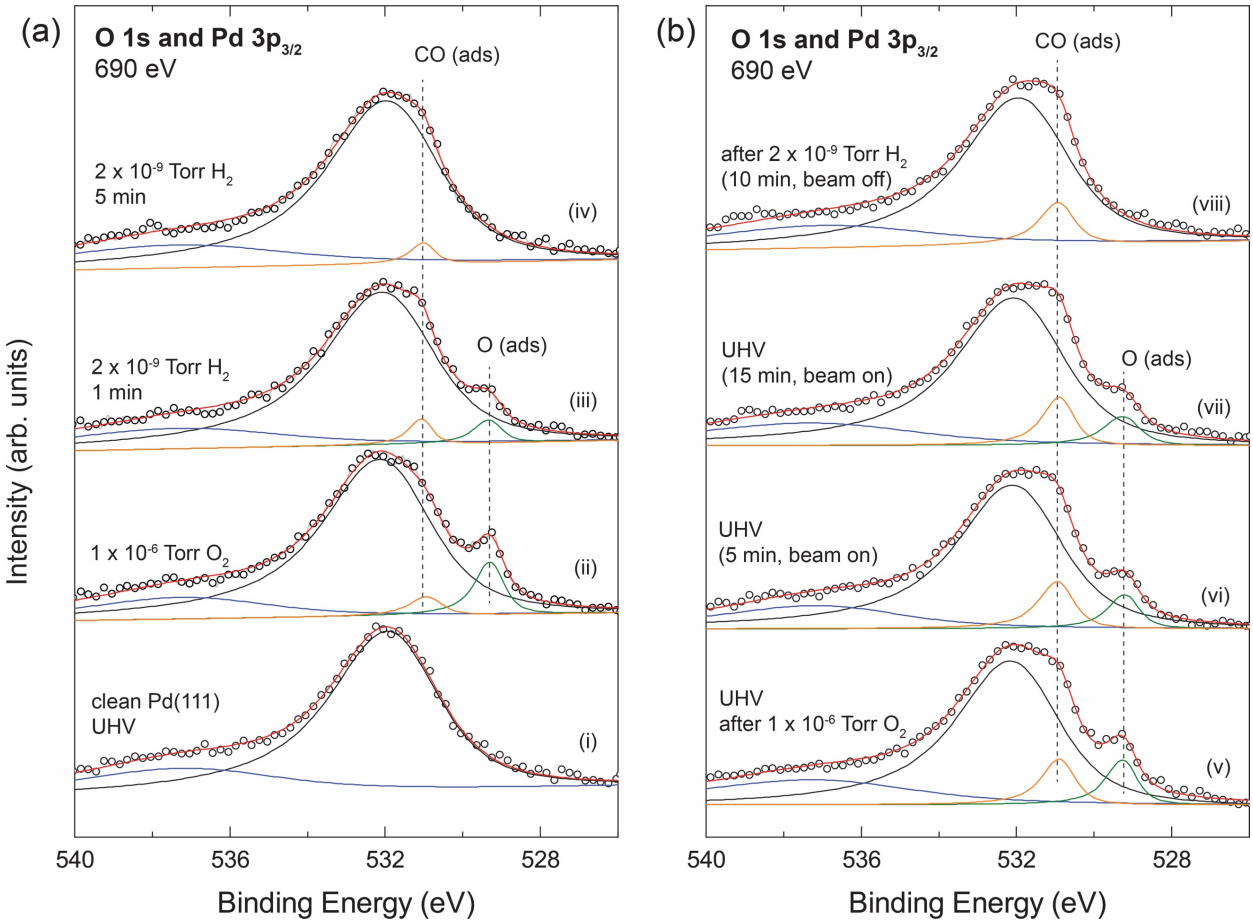


**Figure 4.** (a) O 1s / Pd $3p_{3/2}$ XPS spectra of (i) clean Pd(111) in UHV, (ii) after introducing by 1 × $10^{-6}$ Torr of $O_2$ to prepare chemisorbed O, followed by $O_2$ pump down and (iii) 1 min and (iv) 5 min exposure to 2 × $10^{-9}$ Torr of $H_2$. (b) After the experimental sequence in (a), the sample was (v) re-exposed to 1 × $10^{-6}$ Torr of $O_2$, then spectra were measured after (vi) 5 and (vii) 15 min in UHV with constant exposure to the X-ray beam, and finally (viii) after exposure to 2 × $10^{-9}$ Torr of $H_2$ without X-ray beam exposure and pumped down.

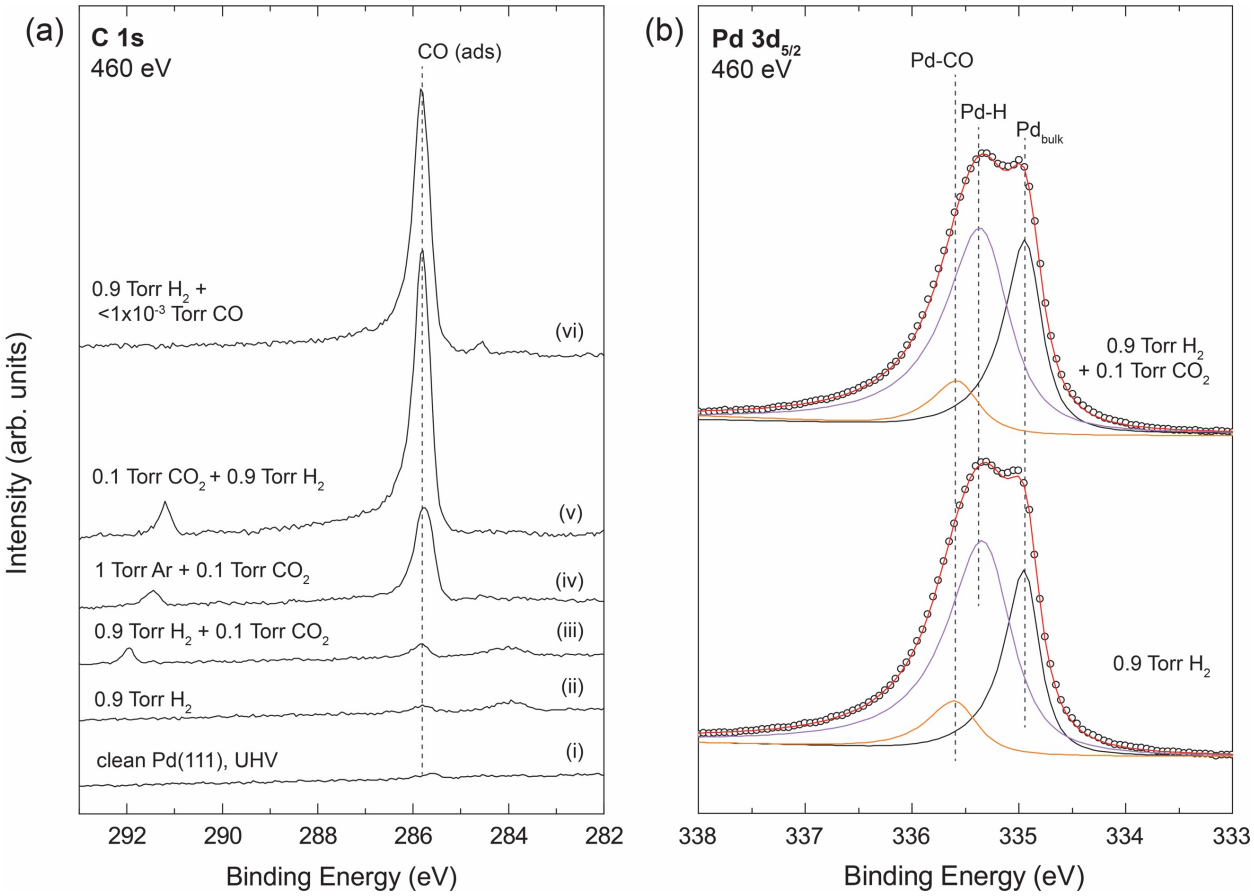


**Figure 5.** (a) C 1s XPS spectra of Pd(111) (i) clean in UHV, (ii) in 0.9 Torr of $H_2$, (iii) after adding 0.1 Torr of $CO_2$ to 0.9 Torr of $H_2$, (iv) 1 Torr of Ar followed by 0.1 Torr of $CO_2$, (v) with 0.1 Torr of $CO_2$ introduced first followed by 0.9 Torr of $H_2$, and (vi) with 0.9 Torr of $H_2$ first followed by less than 1 x $10^{-3}$ Torr of CO. (b) Pd $3d_{5/2}$ XPS spectra of Pd(111) in (bottom) 0.9 Torr of $H_2$ (corresponding to spectrum (ii) in (a)) and (top) in 0.9 Torr of $H_2$ followed by 0.1 Torr of $CO_2$ (corresponding to (iii) in (a))

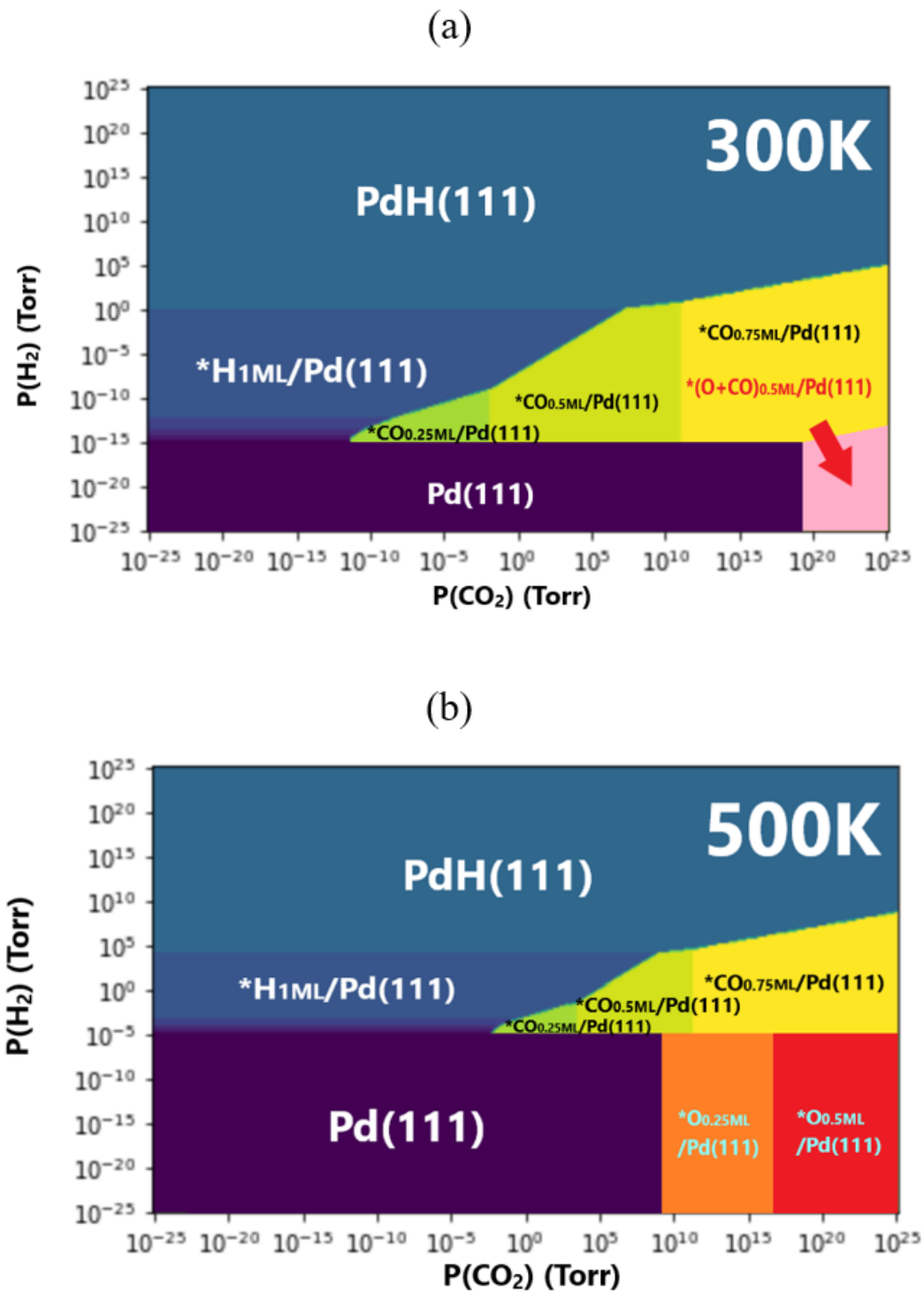


**Figure 6**. Pd(111) phase diagram at 300 (a) and 500 K (b) depending on the partial pressures of $CO_2$ and $H_2$. The phases between Pd(111) and *$H_{1ML}$/Pd(111) corresponded to the Pd(111) surfaces with gradually incremental coverage of *H

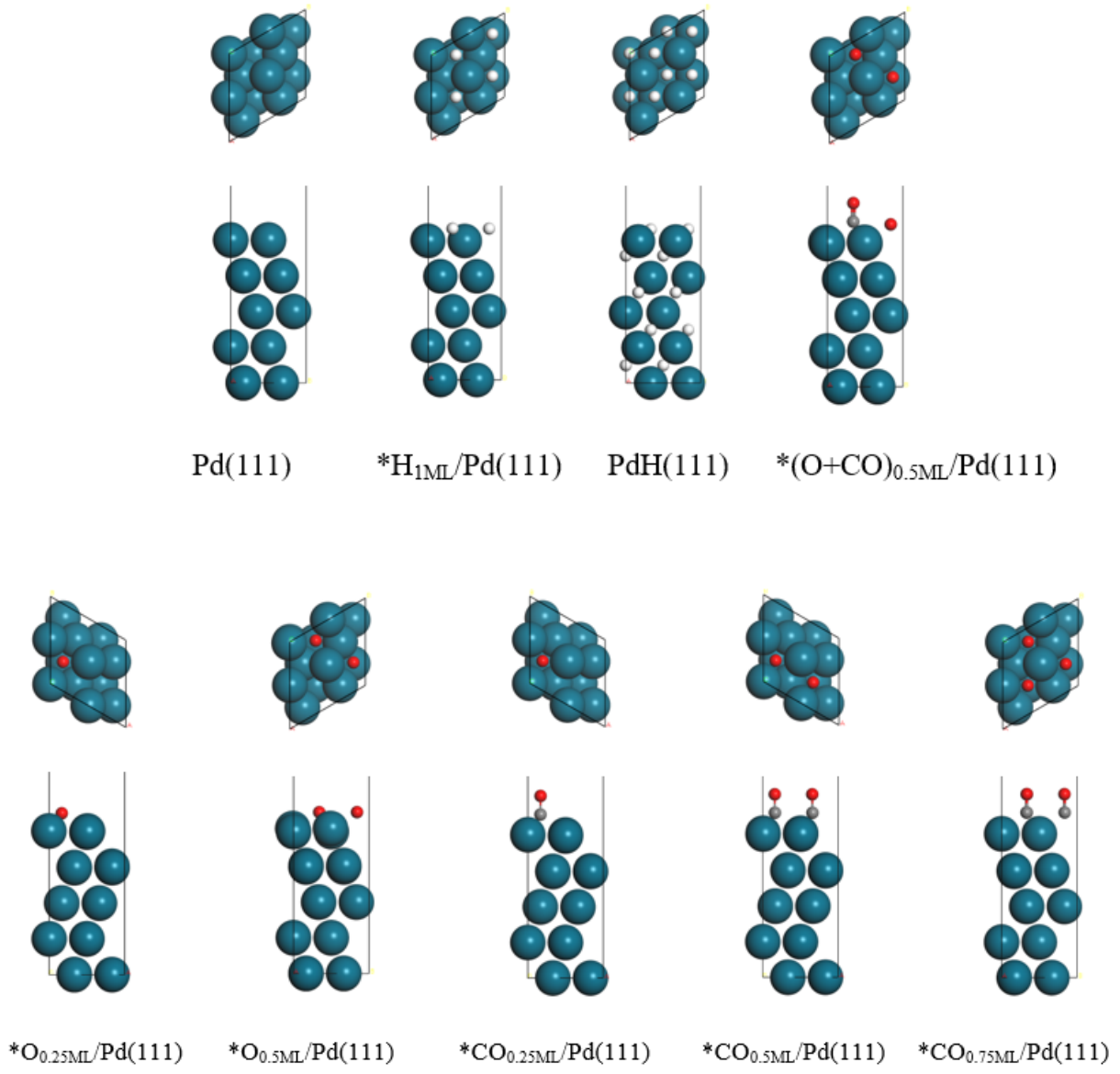


**Figure 7**. DFT-optimized structures of the surfaces (top/side views) shown in Figure 6 (Blue: Pd, White: H, Grey: C, Red: O).

## TOC Graphic